Nano-scale modification of 2D surface structures exposed to 6 keV carbon ions: experiment and modeling

Andreas Mutzke[1], Ivan Bizyukov[2,4], Ralf Schneider[3], James Davis[4]

[1] *Max-Planck-Institut für Plasmaphysik, EURATOM Association, Wendelsteinstr. 1, 17491 Greifswald, Germany*
[2] *Karazin Kharkiv National University, Faculty of Physics and Technologies, 31 Kurchatov Ave., Kharkiv 61108, Ukraine*
[3] *Institute of Physics, Ernst-Moritz-Arndt University, Felix-Hausdorff-Str. 6, 17489 Greifswald, Germany*
[4] *University of Toronto Institute for Aerospace Studies, 4925 Dufferin Street, Toronto, Ontario, Canada M3H 5T6*

Abstract

In this work, a Si pitch grating with typical lateral dimensions of 200-250 nm was exposed to 6 keV C^+ ions at normal incidence and at an angle of 42° both parallel and perpendicular to the grating structure. In contrast to volatile and recycling ions (like Ar^+ or H^+), non-recycling ions are able to modify the surface not only due to sputtering, but also due to implantation of incident ions and the re-deposition of projectile atoms following sputtering or reflection. The target-projectile combination used in this work is an example of such a system forming a mixed Si-C surface. The interaction between the ion beam and the surface has been studied both experimentally and numerically with the focus on validation of the numerical model of the newly developed SDTrimSP-2D code. SDTrimSP-2D is capable of following the evolution of the Si-C system including ion-surface interactions with 2D micro- and nano-structured surfaces. The SDTrimSP-2D code takes the interdependency of surface morphology, sputtering and implantation into account. The simulated surface morphology has been compared to cross-sections of bombarded Si pitch grating obtained by SEM, revealing good agreement between experiment and simulation. The calculations also provide improved insight into the mechanisms of surface modification by sputtering, implantation and material transport by redeposition.

Keywords: SDTrimSP-2D, sputtering, implantation, redeposition, surface morphology, local ion-surface interactions.

PACs numbers: [reserved for the case if needed]

1. Introduction

Sputtering of a surface exposed to a flux of energetic ions is one of the most studied effects of ion-surface interactions [1]. However, the details of ion-surface interactions depend greatly on the target-projectile combination. In cases where the projectile is an ion of a volatile (recycling) element, sputtering is usually the dominant process and the surface is eroded. In such cases, experiments are well described theoretically, at least for relatively smooth surfaces. The sputtering yield is the main parameter, which has been used to validate theoretical models with experiments. Existing models like the TRIM code show good agreement with experiment for many target-projectile combinations.

If the projectile is a non-recycling (non-volatile) ion, its interaction with the surface can lead to implantation, if the ion, after penetration and deceleration in the solid, remains in the surface. This leads to the formation of a mixed surface of target and projectile atoms. The properties of the mixed surface may differ significantly from the properties of the original materials [3]. Additionally, the surface composition may be continuously changed by further sputtering and implantation. The study of such interactions cannot be described simply by the sputtering yield behavior; it is strongly dependent on the elemental composition of the surface, which, in turn, is modified continuously by the ion bombardment. Similar difficulties are encountered, when volatile ions interact with compounds or a surface is exposed to the mixed flux of volatile and non-recycling ions [4]. To solve this problem, a dynamic version of the TRIM code, called TRIDYN [5] (later re-written as SDTrimSP [6]) was developed. This is a 1D version of TRIM, where the distance from the surface into the solid is discretized on a grid and dynamical change of the surface composition along the depth due to implantation of projectiles and relocation of recoils during collisional cascades are considered. There were a number of studies comparing experiments with TRIDYN simulations showing generally good agreement; a summary of these comparisons is published in [2].

The existing models assume that a plane and perfectly smooth surface exists and demonstrate good agreement with experiments, if well polished specimens are used. However, surface roughness is prone to increase the sputtering yield up to a factor of 5. There have been a few approaches to predict the sputtering yields of rough surface: Ruzic suggested considering the surface roughness as having a fractal geometry [7]; Kuestner *et.al.*, assumed that the surface can be represented as aggregates of simple surfaces at tilted angles [8,9]. These approaches yield results in reasonable agreement with experiments, but their intrinsic limitations had prevented further development of the models. One key limitation is the inability to simulate surface morphology changes resulting from deposition and implantation.

This limitation can be overcome by extending the grid of the existing model into the second and third lateral dimensions. The first step in this direction has been implemented in the SDTrimSP-2D code [10], which is capable of treating the interaction of ions with a 2D surface. The code belongs to the TRIM family and it incorporates the same physical model, but due to the second lateral dimension, it requires an advanced relaxation mechanism. We have already shown that the code can predict the evolution of a Si pitch grating exposed to 6 keV Ar^+ ions with good accuracy [11]. Although this system does not have the complications associated with non-recycling, the agreement between the experiment and numerical simulation demonstrates the validity of the basic physics included in the model. We have also previously looked at the C^+ bombardment case in a situation (42^o parallel to the structure) dominated by sputtering [11a]. In

addition, the code has been used to evaluate the effect of the surface roughness on W exposed to C^+ [12] and C^++D^+ fluxes [13].

In this work, we use 6 keV C^+ ions instead of volatile 6 keV Ar^+ ions. The structure is bombarded at normal incidence as well as at angles of 42° both parallel and perpendicular to the structure (Figure 1). This study tries to clarify the different contributions of sputtering, implantation and deposition. Similar to previous work [11, 11a], the cross-sections of the modified Si pitch grating structures obtained with scanning electron microscope (SEM) are compared to those obtained by simulations. The calculations provide insight into local sputtering, implantation and deposition on the scale of a few 100 nm, which is not available with currently existing experimental diagnostics.

2. Experimental procedures

The experimental procedure is very similar to that described in [11]. Figure 2(a) shows a typical SEM image of the initial state of the pitch grating cross-section, i.e. before any exposure. The specimen with nano-scale grating is fabricated on a Si wafer with an intermediate Ta layer with a thickness of 650 nm. The Ta layer has been introduced as a reference marker to allow quantitative measurements of the erosion. The period of the structure has been designed to be 500 nm (250 nm for pits and 250 nm for grates); the height of the grates is 200 nm. The actual grating dimensions deviate from the nominal values by 5-20 nm, which imposes a lower limit on the agreement between the experimental results and calculations. Although the code can accept any surface profile as initial condition, the nominal structure parameters were used because they are considered to be a representative average. Typical differences between the specimen cross-section and the initial surface profile used in simulations are shown in Figure 2 (b).

The pitch grating specimens were irradiated in the UTIAS dual-beam mass-separated ion accelerator [14] with a beam of 6 keV C^+ ions. The angle of incidence was fixed to be either perpendicular to the macroscopic plane of the specimen, or at an angle of 42°. The bombarded area was partly covered with aluminum foil to provide an untouched surface adjacent to the irradiated one, providing a sharp transition from the virgin surface to the exposed one.

The experimental fluence was derived from a measurement of the ion beam current and the beam spot area. The ion beam current was 1 μA over a beam spot with typical diameter of 4-5 mm at normal incidence, such that the average flux was $\approx 0.5\times10^{18}$ $m^{-2}s^{-1}$. For the experiment at normal incidence, the fluence was $50\text{-}100\times10^{20}$ m^{-2}; at tilted angles the fluence was $10\text{-}20\times10^{20}$ m^{-2}. Since the beam spatial distribution is expected to be approximately Gaussian, strong variations in flux and fluence are expected across the exposed area, and particularly towards the periphery of the exposed region.

Following the bombardment, the specimens were extracted from the vacuum system and cracked to achieve the cross-sectional view. The cross-section was studied using a high-resolution Hitachi S-5200 Scanning Electron Microscope.

A series of cross-sections after ion exposure, together with the simulated surface profiles, is shown in . These show the evolution of the surface morphology under ion bombardment. The SEM measured the signal of back-scattered electrons. This mode is more sensitive to the elemental composition of the surface, rather than relief, allowing separation of native Si structure from that created by C deposition and implantation. Note that the SEM images were taken outside the region immediately adjacent to the Al foil to avoid contributions from redeposited Al atoms to the evolution of the surface morphology. The variations observed in the surface modification are due to the non-uniform (Gaussian) beam profile, where the ion current density

is gradually reduced towards the edges of the irradiated spot. As a result, the central part of the bombarded surface is irradiated with a higher fluence, while edges are less exposed. Thus, fracturing the specimens along the diameter of the beam spot produced a cross-section of the surface with varying ion beam exposure. Using SEM, a series of cross-section images were taken at different locations (i.e. at different radii of the spot) experiencing different fluences.

3. The SDTrimSP-2D program

SDTrimSP-2D [10] is a 2-D extension of SDTrimSP [6], which, in turn, is a generalized version of the TRIDYN program [5]. It can be run in static or dynamic mode (SD) on sequential or parallel systems (SP). SDTrimSP-2D uses a 2-D mesh to represent the surface morphology, the first dimension is the direction perpendicular to the macroscopic surface plane, and the second is in a direction parallel to that plane. This representation is sufficient to simulate the ion bombardment of surfaces with 2D micro-structure extended into the 3rd dimension. It shares the same physical model of ion-surface interactions with other codes of the TRIM family. However, the resolution of a second dimension requires a 2-D domain with separate cells.

The code follows the density changes in the target material due to projectile and recoil particles coming to rest after a complete slowing-down at the end of their trajectories. In SDTrimSP/TRIDYN, this is done by a 1-D relaxation of the cells. Each trajectory creates a mass flux in the cells it passes. These fluxes can act as sink or source terms for the particle densities. To ensure particle conservation within the numerical setup, which uses a 1D grid of cells in which each cell has a constant volume density according to the material, volume changes of the 1D cells (expansion or contraction perpendicular to the surface) are used to represent changes to the number of particles in a cell. In SDTrimSP-2D, this procedure has been extended to 2D, subject to the requirement that all volume changes applied are divergence free. This reflects particle conservation in the projectile-target system expressed by volume changes. For each cell, the resulting mass fluxes (representing the transfer of particles into or out of the cell) are taken to be anisotropic by introducing the anisotropy coefficient (K_{anis}) of the volume relaxation. This anisotropy coefficient defines the ratio of horizontal volume changes (representing horizontal mass fluxes parallel to the surface) and perpendicular volume changes (representing mass fluxes in vertical direction). The horizontal transport (parallel to the surface) is usually set smaller than the vertical one, because swelling or shrinking are primarily observed experimentally in the vertical direction. In the simulations presented here an anisotropy coefficient of 0.5 was used. Thus, the cells at the surface exposed to incident ions can change in two directions. The volume of cells without sides bordering on the surface is kept fixed. The relaxation process is done in several iterations until the divergence of the mass fluxes (transfer of particles between cells) becomes zero and steady-state conditions without internal tension are obtained. From this steady-state, divergence-free solution the volume changes are applied. In addition, splitting and annihilation of cells was introduced in SDTrimSP-2D, according to a maximum and minimum number of atoms, to be able to represent creation of holes or strong deposition.

Since the surface is a periodic structure in the lateral direction, periodic boundary conditions in this direction are used.

Additional diagnostics are used to analyze the results of the numerical computations and are able to provide local values of the sputtering and redeposition yields. The local sputtering yield is defined as the number of surface atoms $N_{sputter}$ removed from a given cell normalized to the number of incident C atoms $N_{incident}$. For a given surface cell, it is calculated as

$Y = N_{sputter}/N_{incident}$

Note that surface atoms lost from one cell may end up in another or may pass through several cells before reaching the surface. Similarly, incident C^+ ions may have first passed through other cells.

To keep track of these events, we use three different sputter yields: Y_{local} and $Y_{removed}$. For the calculation of Y_{local}, the number of particles counted as sputtered surface atoms is measured at some distance away from the surface to exclude those particles which are redeposited. For $Y_{removed}$ all particles removed from the surface are taken into account, independent of their subsequent paths; thus, redeposited particles are also included.

Similar to the sputtering yield, the redeposition "yield" calculates the number of all previously sputtered Si atoms passing through the surfaces of a cell, $N_{implanted}$, again normalized to the number of incident C atoms in this cell $N_{incident}$. It is calculated as:

$Re_{local} = N_{implanted}/N_{incident}$

Both values refer to all particles travelling through a given local cell at the surface. Atoms may ultimately be deposited deeper in the material, however, such a deposition event is counted in the local redeposition yield only for the cell through which it has penetrated into the specimen. All incident C atoms are also accounted for in the same way.

The introduction of the two yields, Y_{local} and $Y_{removed}$ is useful in the analysis of the particle transport effects. The sources of redeposited particles are cells at which $Y_{removed} - Y_{local} > 0$, and the larger the difference between these two yields the stronger the contribution to the redeposition. The particles are transported to and redeposited on surfaces with $Re_{local} > 0$; net deposition occurs on surfaces for which $Re_{local} > Y_{removed}$.

4. Results and discussion

4.1 Bombardment at normal incidence

The comparison of experiment and simulation is shown in for a series of fluences. The simulated surface profiles (actually the top surface of the structure and the layer of C in Si with concentration of 20 at.%) are overlaid in red on the SEM photos. In the vertical planes of Figure 3, the bottom of the square has been matched to the interface between the Ta layer and the Si grating; in the horizontal plane the vertical axes of symmetry were aligned.

The exposure leads to C deposition on the surfaces normal to the C ion flux. One can see that with increasing fluence the thickness of the carbon deposit increases and the features of the structure become narrower. Moreover, the elemental composition of the deposit changes from pure Si to C/Si. On horizontal surfaces, a layer of implanted C develops and protects the Si from further sputtering. Over the range of simulated fluences, the calculations show very good agreement with experiments and provide an accurate progression of the surface structure within the initial accuracy of the pitch grating structure, 10 – 20 nm.

The thickness of the C deposition on planar surfaces of the structure can be compared with the case of C ions interacting with a plane 1-D Si surface. The calculated 1-D C profiles for such a case are shown in Figure 4. The thickness of C deposition (measured at the point, where C elemental concentration is 20 at.%) is very similar for 1-D and 2-D (plane surfaces only) cases. Differences between the structured and plane surface appear only at inclined surfaces. Moreover, the exchange of the atoms between inclined and horizontal surfaces in the structure (due to sputtering, reflection and re-deposition) appear to nearly compensate each other and does not contribute to the thickness of the C overlayer.

While the experimental ion fluences cannot be determined at individual points within the beam spot area, the calculated fluences ($35\text{-}105\times10^{20}$ m^{-2}) are consistent with those of the

experiment, 50-100×10^{20} m^{-2} in the central region of the beam spot and lower towards the edges. This consistency provides an independent validation of the sputtering yields calculated by the model.

Thus, the model exhibits excellent agreement between the experimental and calculated surface profiles. It can further be used to reveal details of the dynamics of ion-surface interactions, which are not accessible experimentally. shows a series of calculated surface profiles and the respective sputtering and redeposition yields. Comparing them, one can see the relationship between macro- and nanoscale dynamics of the ion-surface interactions. In general, surfaces with a larger angle of incidence are sputtered more, as indicated by $Y_{removed}$ and, therefore, give the largest contribution to the total sputtering yield. This leads to a narrowing of the structure, because its top is protected by the C layer. The horizontal parts of the structure are already covered with C at a fluence of 30×10^{20} m^{-2}, so the Si is not sputtered from these parts any more. The only source of sputtered Si atoms is the steep side part of the grid, where its concentration gradually decreases from 80 at. % to 30 at. %.

4.2 Bombardment at an angle of 42° parallel to the structure

Incidence of C ions at an inclined angle parallel to the structure produces a surface, which is similar to the structure developing using 6 keV Ar ions [11], and some of the following comparisons were presented in [11a]. At such an inclined angle of incidence, C^+ ion bombardment at this energy results in erosion rather than in deposition, making it similar to the Ar ion irradiation case. The structure, exposed to such a bombardment, evolves towards a triangle shaped form as shown in . The matching of the simulated profiles to the experimental ones in the plots has been performed as described in the previous subsection.

The fluence required by the simulation is 5-55×10^{20} m^{-2}. 55×10^{20} m^{-2} is a reasonable estimate of the maximum experimental fluence at the centre of the beam spot. Average values of the experimental fluence provides are about 10-20×10^{20} m^{-2}, with peak values perhaps 2-3 times larger.

Again, the code is able to follow the evolution of the surface profile with an accuracy of <20 nm. Although the code has been developed to work with 2D micro structured surfaces, the trajectories of projectiles and recoils are all calculated in 3D, giving a correct simulation of sputtering and redeposition. While the surface structure initially has a rectangular shape, for a fluence larger than 40×10^{20} m^{-2} it becomes a trapezium. With further bombardment, the trapezium-shaped structure is retained, but its size decreases.

Local sputtering and redeposition yields are shown in . The erosion occurs at all surfaces, because the C implantation does not turn into a deposition regime creating an overlayer, leaving some Si atoms at the surface for sputtering. Similar to the previous case, the erosion rate is highest at the surface parts with the larger inclinations during the bombardment process. C and Si atoms are both transferred from one side of the structure by sputtering and rejection to another by redeposition. The local angle of incidence always stays above 42°, resulting in higher sputtering yield of both Si and implanted C atoms. Sputtered atoms are transferred from the side walls of the features down to the dip between them. Generally, the transfer patterns are similar to those observed in [11].

Although not observed in the experiment, calculations show that as the fluence increases, the feature is further eroded to become triangular in shape at a fluence of ≈75×10^{20} m^{-2} and

disappears almost completely at a fluence of ≈150×10^{20} m^{-2} [15]. The irradiation ultimately leaves a smooth, mixed Si-C surface.

4.3 Bombardment at an angle of 42° perpendicular to the structure

While the previous two cases have provided examples of symmetrical spatial distributions of sputtering and redeposition, bombardment at an inclined angle perpendicular to the structure will produce strongly asymmetrical profiles. In this case, the structure is modified to a scalene triangle. As seen in the code is again able to follow the complex evolution of the profile. The code has reproduced the observed deposition of implanted C atoms on the right side of the feature. The ion flux polishes the left side of the feature by sputtering at shallow incidence angles, while the right side is smoothed by C implantation. We note that we have performed the simulation using an incidence angle of 37° for better match between the experimental and simulated data; this is within the experimental accuracy of the angle measurement.

Similar to Section 4.2, the experimental and calculated fluencies are consistent, taking into account the non-uniformity of the ion beam intensity, which peaks at the center. An average value of ≈20×10^{20} m^{-2} is again somewhat lower than that required by the simulation (55×10^{20} m^{-2}).

The spatial distribution of the sputtering and redeposition yields in relation to the actual profile is shown in . There are two characteristic peaks at a fluence of 10×10^{20} m^{-2}. The peak on the left part corresponds to sputtering from the left side of the feature. This part of the grating structure is actually shadowed from the direct incidence of beam ions, but sputtering and implantation occurs due to ions reflected from the right part of the feature. As the fluence increases (30×10^{20} m^{-2}), the C implantation process tends to produce a carbon overlayer on top of the right part of the feature, with a corresponding increase of the C redeposition yield. The highest Si sputter yield is observed at the inclined surface located near a position of -100 nm, where the local incidence angle of C ions has its maximum. Further increase of the fluence up to 55×10^{20} m^{-2} produces a thicker and smoother C overlayer on top of the right part of the feature, while the left side is smoothed and tilted due to the shallow-angle sputtering. Both processes act to re-shape the original rectangular structure into a triangular one.

These results can be compared with those obtained in [11] for the same structure bombarded at the same incidence angle, but with 6 keV Ar^+ ions. A similar-looking triangular structure is formed, but without a deposited overlayer. The shape of the line representing 20 at. % C or Ar concentration in the Si is similar for both C^+ and Ar^+ bombardment. In comparison to volatile ion bombardment; the difference between the irradiation with volatile and non-volatile ions is the deposition of implanted atoms at the surfaces, where the local angle of incidence is close to normal.

5. Conclusions

The interaction of 6 keV C^+ ions with a Si pitch grating structure was studied experimentally and by means of numerical simulation using the SDTrimSP-2D code. The pitch gratings were bombarded at normal incidence as well as at an angle of 42°, both parallel and perpendicular to the structure. The evolution of the surface morphology (i.e. cross-sections of the specimens), observed in experiment by SEM operated in a mode sensitive to elemental composition, has been compared to the results of the simulation. In all three cases, this

comparison has shown good agreement between the experimental and simulated profiles within the typical experimental initial deviation of 5-20 nm. The comparison has included the dynamics of the overlayer consisting of implanted C. The simulated results allowed a detailed description of the nanoscale processes accompanying the erosion: local sputtering, deposition and implantation of C ions, redeposition, and transport of the sputtered Si and C atoms from one surface to another.

In this paper we have shown that the SDTrimSP-2D code produces a valid simulation of the interaction of non-recycling ion fluxes with 2D surfaces. The comparison still contains some uncertainty with regard to the absolute sputtering yields and areal densities of implanted C atoms, as the spatial variations in ion fluence can only be estimated from the measurements of beam current and spot size. However, estimates of the variations in fluence over the beam spot are consistent with the values required by the calculations, providing a reasonable independent verification. This question will be addressed in future work, where the fluence dependent sputtering yields will be compared to those calculated by the SDTrimSP-2D code.

Acknowledgements

Authors would like to thank Dr. I. Gourevich from Center for Nanostructure Imaging, Department of Chemistry, University of Toronto. Authors would like to thank Dr. K. Krieger, Materials Research Division, IPP Garching, for helpful discussions in sample design and providing the samples used in this study. Financial support for the experimental work performed at the University of Toronto was provided by the Natural Sciences and Engineering Research Council of Canada through a grant to Prof. A.A. Haasz.

References

1 R. Behrisch (ed). *Sputtering by Particle Bombardment. I. Physical Sputtering of Single-Element Solid*. ISBN 978-3-540-10521-3 (Berlin, Springer, 1979).

2 R. Behrisch, W. Eckstein (ed). *Sputtering by Particle Bombardment. Experiments and Computer Calculations from Threshold to MeV Energies*. ISBN 978-3-540-44500-5 (Berlin, Springer, 2007).

3 R. Behrisch (ed). *Sputtering by Particle Bombardment. II. Sputtering of Alloys and Compounds, Electron and Neutron Sputtering, Surface Topography*. ISBN ISBN 978-3-540-12593-8 (Berlin, Springer, 1983).

4 I. Bizyukov, K. Krieger. *Transition from tungsten erosion to carbon layer deposition with simultaneous bombardment of tungsten by helium and carbon*. J. Appl. Phys. vol.**101**, 104906, (2007).

5 W. Moeller, W. Eckstein, and J. P. Biersack. *TRIDYN - binary collision simulation of atomic collisions and dynamic composition changes in solids*. Comput. Phys. Commun. vol.**51**, pp. 355-368, (1988).

6 W. Eckstein, R. Dohmen, A. Mutzke, and R. Schneider. *SDTrimSP: A Monte-Carlo Code for Calculating Collision Phenomena in Randomized Targets*. IPP Report 12/3 (Garching, Max-Planck-Institute for Plasmaphysics, 2007).

7 D. Ruzic. *The effects of surface roughness characterized by fractal geometry on sputtering*. Nucl. Instrum. Meth. vol.**B47**, pp. 118-125, (1990).

8 M. Kuestner, W. Eckstein, V. Dose, and J. Roth. *The influence of surface roughness on the angular dependence of the sputter yield*. Nucl. Instrum. Meth. vol.**B145**, pp. 320-331, (1998).

9 M. Kuestner, W. Eckstein, E. Hechtl, and J. Roth. *Angular dependence of the sputtering yield of rough beryllium surfaces*. J. Nucl. Mater. vol.**265**, pp. 22-27, (1999).

10 A. Mutzke, R. Schneider. *SDTrimSP-2D: Simulation of Particles Bombarding on a Two Dimensional Target Version 1.0*. IPP Report 12/4 (Garching, Max-Planck-Institute for Plasmaphysics, 2009).

11 I. Bizyukov, A. Mutzke, R. Schneider, and J. Davis. *Evolution of the 2D surface structure of a silicon pitch grating under argon ion bombardment: Experiment and modeling*. Nucl. Instr. and Meth. vol.**B268**, pp. 2631-2638, (2010).

12 I. Bizyukov, A. Mutzke, R. Schneider, A. Gigler, and K. Krieger. *Morphology and changes of elemental surface composition of tungsten bombarded with carbon ions*. Nucl. Instrum. Meth. vol.**B266**, pp. 1979-1986, (2008).

13 A. Mutzke, R. Schneider, and I. Bizyukov. *SDTrimSP-2D studies of the influence of mutual flux arrangement on erosion and deposition*. J. Nucl. Mater. vol.**390-391**, pp. 115-118, (2009).

14 J. W. Davis, A. A. Haasz. *Synergistic chemical erosion of graphite due to simultaneous bombardment by H+ and other low-Z ions using a dual-beam accelerator*. Nucl. Instrum. Meth. vol.**B83**, pp. 117-124, (1993).

15 R. Schneider, A. Mutzke, I. Bizyukov, and J. W. Davis. *Bombardment of a silicon pitch grating by C^+ ions at an inclined incident angle parallel to the structure*, 19th International Conference on Plasma Surface Interactions, San Diego, U.S.A., May 24-28, 2010, accepted for publication in J. Nucl. Mater. doi:10.1016/j.jnucmat.2010.08.064

List of Figure Captions

Figure 1. The direction of the incident ion beam on the pitch grating: (a) – normal angle of incidence, (b) – incidence at an angle of 42° parallel to the structure and (c) – incidence at an angle of 42° perpendicular to the structure.

Figure 2. (a) – SEM image of a cross-section of the Si pitch grating. A silicon wafer (the substrate) is covered by a 650 nm Ta layer; on top of this is the Si pitch grating structure manufactured by means of lithographic methods. (b) – the cross-section of the Si pitch grating in comparison to initial profile used in the simulations.

Figure 3. SEM images of a cross-section of the Si pitch grating following bombardment at normal incidence. Red colored graphs are the surface profiles simulated by SDTrimSP-2D code: the upper solid line is the top surface of the structure, the dashed line is the location where the C concentration is 20 at.%. All scales are given in nanometers. Different images correspond to different incident fluence. The fluence values have been taken from the results of the simulation: (a) – 30×10^{20} m^{-2}; (b) – 65×10^{20} m^{-2}; (c) – 85×10^{20} m^{-2}; (d) – 105×10^{20} m^{-2}.

Figure 4. SDTrimSP calculations of C implantated profiles for a 1-D Si surface as a function of fluence for 6 keV C^+ ions bombarding a plane Si surface at normal incidence.

Figure 5. Calculated surface profiles; Y_{local} (red lines), $Y_{removed}$ (green lines), Y_{static} (black lines) and redeposition (blue lines) yields for different fluence values as a function of position. Colored regions on the profile correspond to the local C elemental concentration. Solid lines on the yield graphs correspond to Si, while dotted lines correspond to C. All scales are given in nanometers.

Figure 6. SEM images of a cross-section of the Si pitch grating following bombardment at an angle of 42° parallel to the structure. Red colored graphs are the surface profiles simulated by SDTrimSP-2D code: the upper solid line is the top surface of the structure, the dashed line is the location where the C concentration is 20 at.%. All scales are given in nanometers. Different images correspond to different incident fluence. The fluence values have been taken from the results of the simulation: (a) – 5×10^{20} m^{-2}; (b) – 15×10^{20} m^{-2}; (c) – 40×10^{20} m^{-2}; (d) – 55×10^{20} m^{-2}.

Figure 7. Calculated surface profiles; Y_{local} (red lines), $Y_{removed}$ (green lines), Y_{static} (black lines) and redeposition (blue lines) yields for different fluence values as a function of position. Colored regions on the profile correspond to the local C elemental concentration. Solid lines on the yield graphs correspond to Si, while dotted lines correspond to C. All scales are given in nanometers.

Figure 8. SEM images of a cross-section of the Si pitch grating following bombardment at an angle of 42° perpendicular to the structure. Red colored graphs are the surface profiles simulated by SDTrimSP-2D code: the upper solid line is the top surface of the structure, the dashed line is the location where the C concentration is 20 at.%. All scales are given in

nanometers. Different images correspond to different incident fluence. The fluence values have been taken from the results of the simulation: (a) – 10×10^{20} m^{-2}; (b) – 30×10^{20} m^{-2}; (c) – 45×10^{20} m^{-2}; (d) – 55×10^{20} m^{-2}. The simulations were done for an incidence angle of 37º to better match the experiment. The beam is incident from the right.

Figure 9. Calculated surface profiles; Y_{local} (red lines), $Y_{removed}$ (green lines), Y_{static} (black lines) and redeposition (blue lines) yields for different fluence values as a function of position. Colored regions on the profile correspond to the local C elemental concentration. Solid lines on the yield graphs correspond to Si, while dotted lines correspond to C. All scales are given in nanometers.

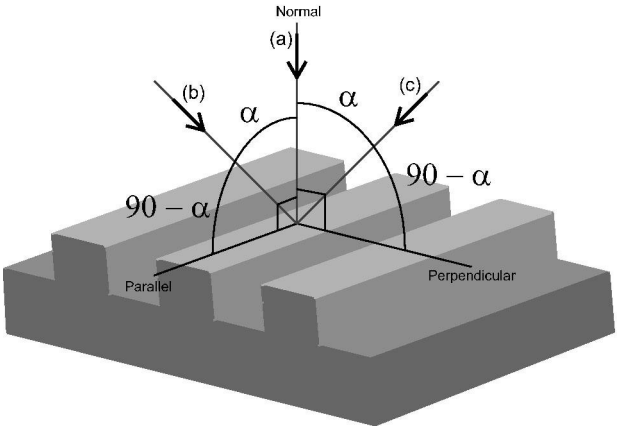

Figure 1

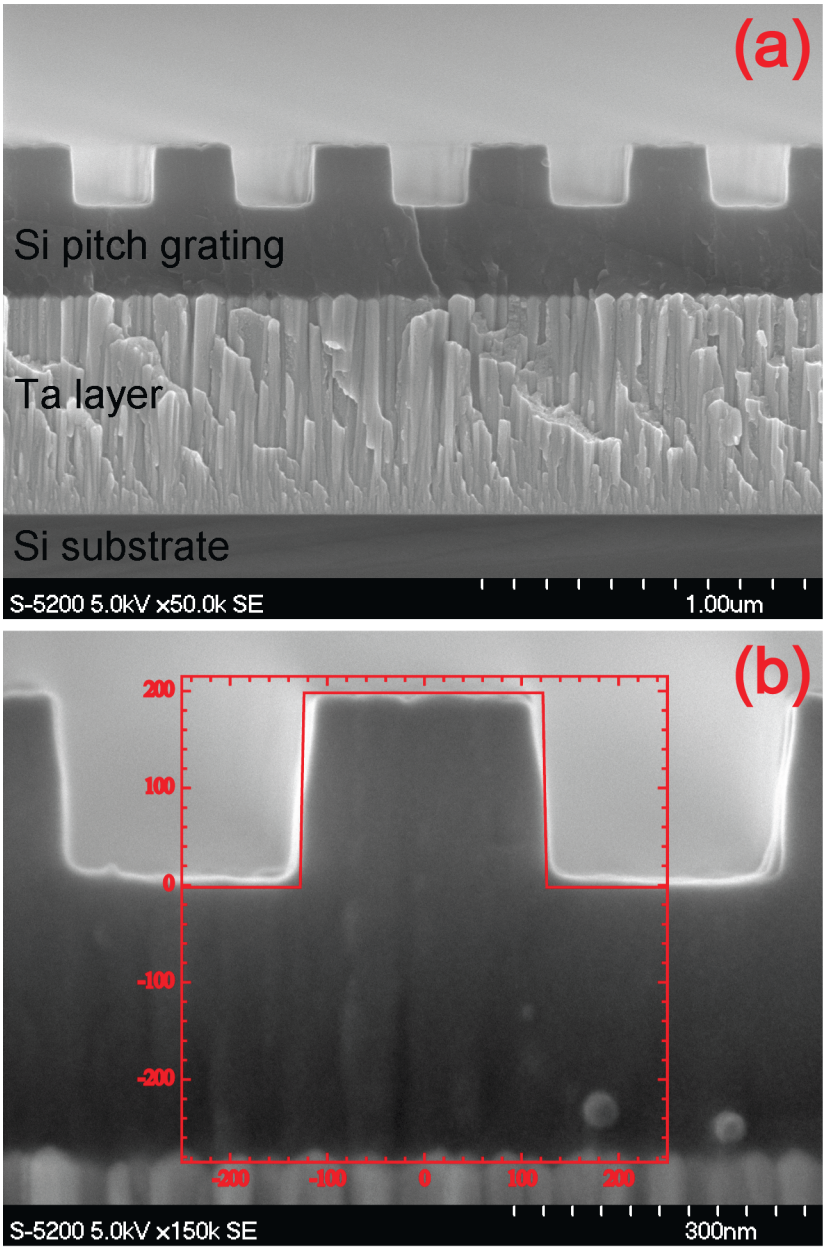
(a)
Si pitch grating
Ta layer
Si substrate
S-5200 5.0kV x50.0k SE
1.00um
(b)
200
100
0
-100
-200
-200
-100
0
100
200
S-5200 5.0kV x150k SE
300nm

Figure 2

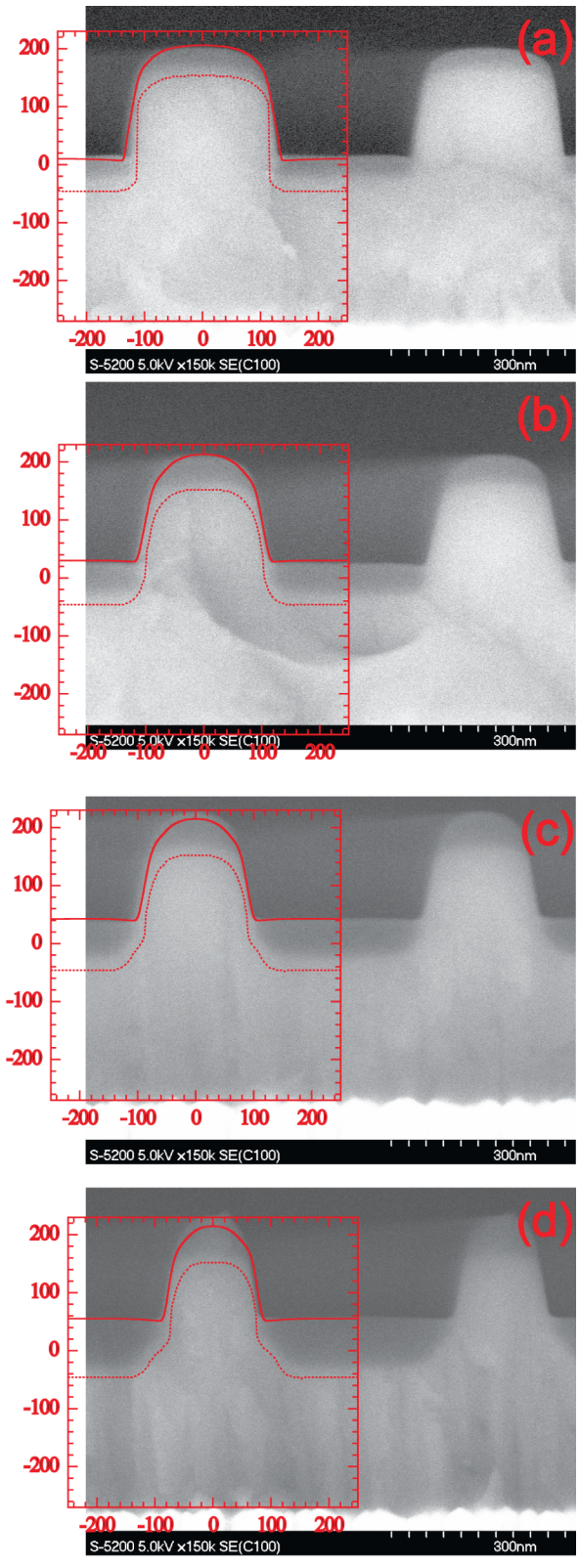
(a)
200
100
0
-100
-200
-200 -100 0 100 200
S-5200 5.0kV x150k SE(C100)
300nm
(b)
200
100
0
-100
-200
-200 -100 0 100 200
S-5200 5.0kV x150k SE(C100)
300nm
(c)
200
100
0
-100
-200
-200 -100 0 100 200
S-5200 5.0kV x150k SE(C100)
300nm
(d)
200
100
0
-100
-200
-200 -100 0 100 200
S-5200 5.0kV x150k SE(C100)
300nm

Figure 3

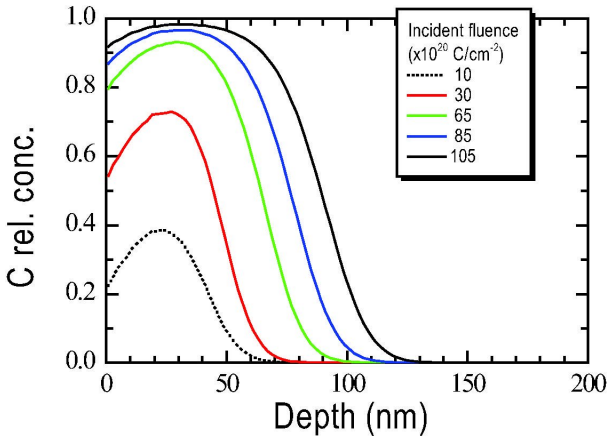

Figure 4

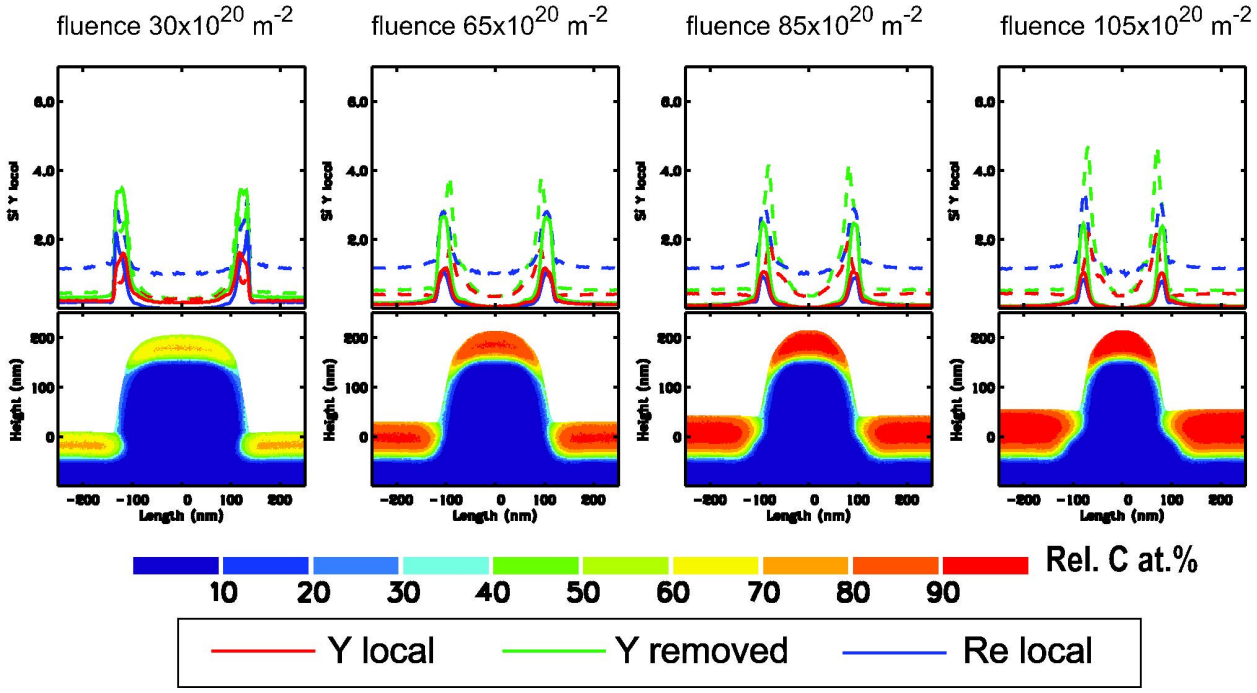

Figure 5

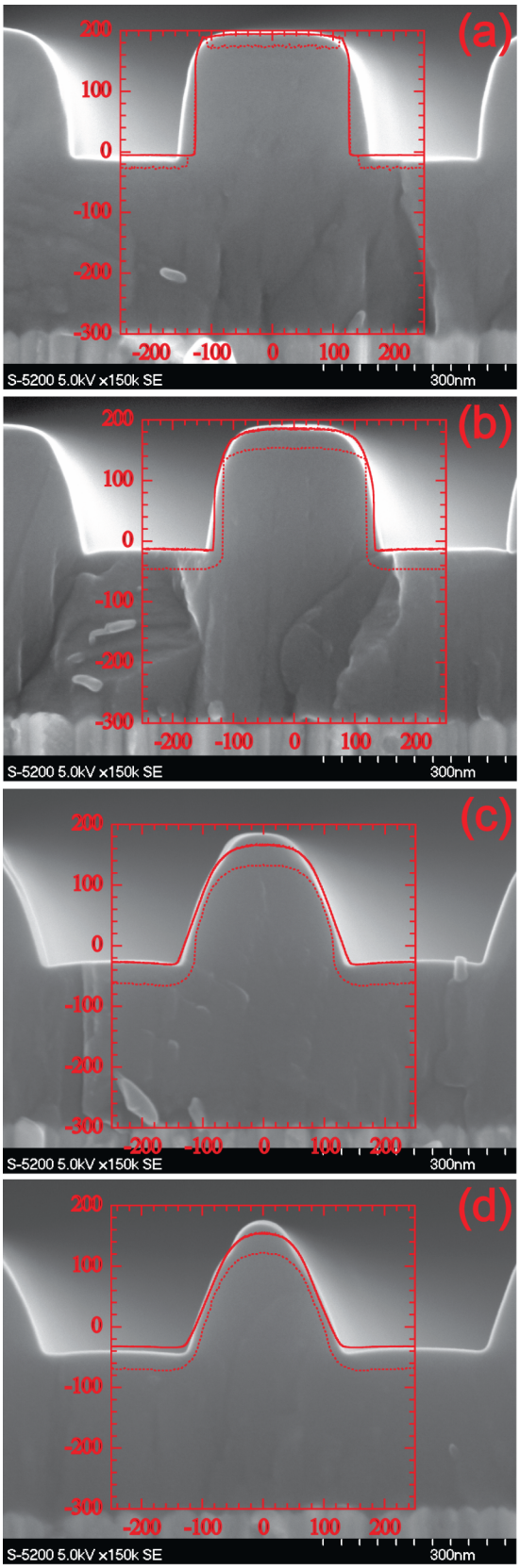
(a)
200
100
0
-100
-200
-300
-200 -100 0 100 200
S-5200 5.0kV x150k SE
300nm
(b)
200
100
0
-100
-200
-300
-200 -100 0 100 200
S-5200 5.0kV x150k SE
300nm
(c)
200
100
0
-100
-200
-300
-200 -100 0 100 200
S-5200 5.0kV x150k SE
300nm
(d)
200
100
0
-100
-200
-300
-200 -100 0 100 200
S-5200 5.0kV x150k SE
300nm

Figure 6

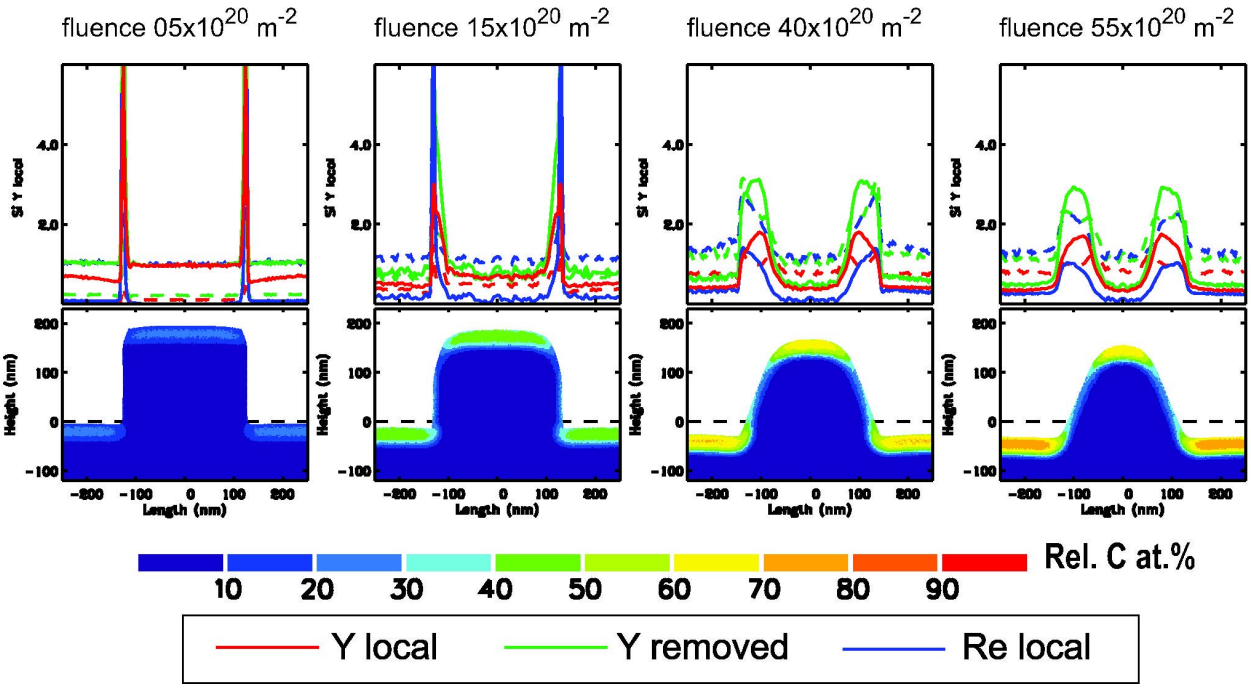
fluence 05x10^20 m^-2
fluence 15x10^20 m^-2
fluence 40x10^20 m^-2
fluence 55x10^20 m^-2
Si Y local
Height (nm)
Length (nm)
Rel. C at.%
10 20 30 40 50 60 70 80 90
Y local
Y removed
Re local

Figure 7

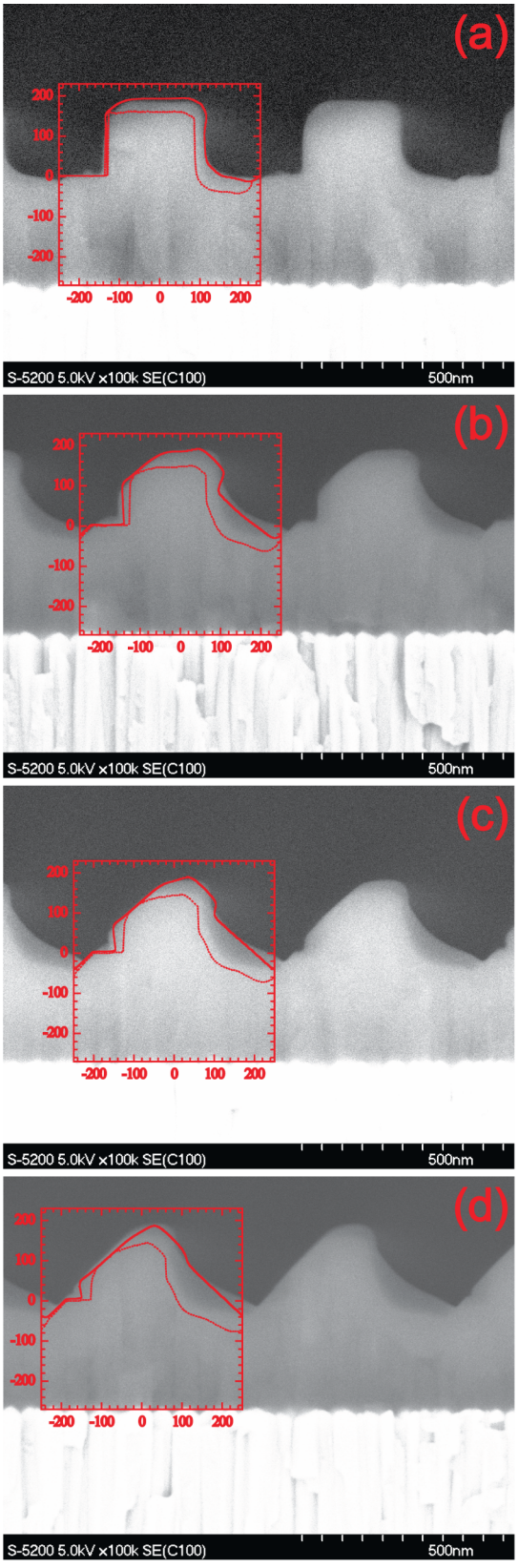
(a)
200
100
0
-100
-200
-200 -100 0 100 200
S-5200 5.0kV x100k SE(C100)
500nm
(b)
200
100
0
-100
-200
-200 -100 0 100 200
S-5200 5.0kV x100k SE(C100)
500nm
(c)
200
100
0
-100
-200
-200 -100 0 100 200
S-5200 5.0kV x100k SE(C100)
500nm
(d)
200
100
0
-100
-200
-200 -100 0 100 200
S-5200 5.0kV x100k SE(C100)
500nm

Figure 8

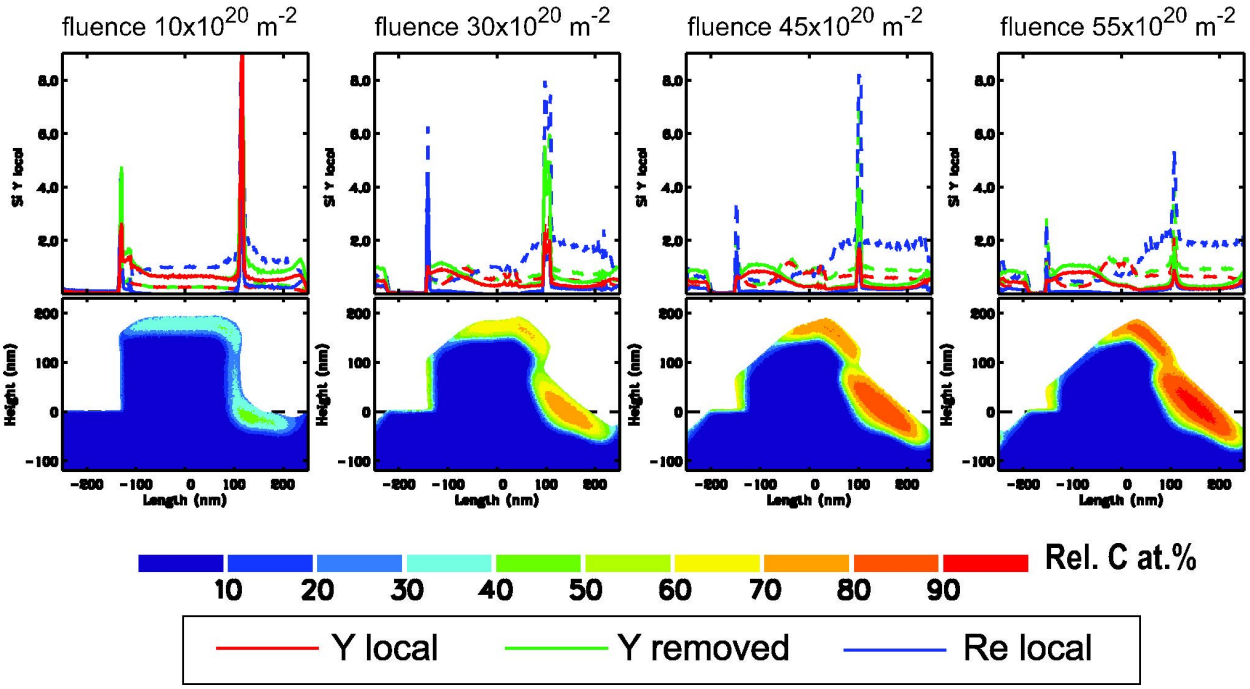
fluence 10x10^20 m^-2
fluence 30x10^20 m^-2
fluence 45x10^20 m^-2
fluence 55x10^20 m^-2
Si Y local
Height (nm)
Length (nm)
Rel. C at.%
10 20 30 40 50 60 70 80 90
Y local
Y removed
Re local

Figure 9